J. Fluid Mech. (1998), *vol.* 369, *pp.* 351–380. Printed in the United Kingdom

© 1998 Cambridge University Press

Supersonic vortex breakdown during vortex/cylinder interaction

By I. M. KALKHORAN[1], M. K. SMART[2] AND F. Y. WANG[1]

[1] Department of Mechanical, Aerospace, and Manufacturing Engineering, Polytechnic University, Brooklyn, NY 11201, USA

[2] NASA Langley Research Center, Hampton, VA 23681, USA

(Received 22 October 1996 and in revised form 2 March 1998)

The head-one interaction of a supersonic streamwise vortex with a circular cylinder reveals a vortex breakdown similar in many ways to that of incompressible vortex breakdown. In particular, the dramatic flow reorganization observed during the interaction resembles the conical vortex breakdown reported by Sarpkaya (1995) at high Reynolds number. In the present study, vortex breakdown is brought about when moderate and strong streamwise vortices encounter the bow shock in front of a circular cylinder at Mach 2.49. The main features of the vortex/cylinder interaction are the formation of a blunt-nosed conical shock with apex far upstream of the undisturbed shock stand-off distance, and a vortex core which responds to passage through the apex of the conical shock by expanding into a turbulent conical flow structure. The geometry of the expanding vortex core as well as the location of the conical shock apex are seen to be strong functions of the incoming vortex strength and the cylinder diameter. A salient feature of the supersonic vortex breakdown is the formation of an *entropy-shear* layer, which separates an interior subsonic zone containing the burst vortex from the surrounding supersonic flow. In keeping with the well-established characteristics of the low-speed vortex breakdown, a region of reversed flow is observed inside the turbulent subsonic zone. The steady vortex/cylinder interaction flow fields generated in the current study exhibit many characteristics of the unsteady vortex distortion patterns previously observed during normal shock wave/vortex interactions. This similarity of the instantaneous flow structure indicates that the phenomenon previously called *vortex distortion* by Kalkhoran *et al.* (1996) is a form of supersonic vortex breakdown.

1. Introduction and review

Understanding the dynamics and behaviour of concentrated streamwise vortices constitutes a problem of fundamental importance in the operational environment of aerospace vehicles. In three-dimensional flows, boundary layer separation leads to formation of concentrated vortical structures which, once away from the surface, convect downstream and may interact with other components of the vehicle. Such interactions are in general undesirable from a performance standpoint as they may lead to increase in drag, loss of lift, alteration of the pitching moment characteristics of the vehicle as well as excessive aerothermal loads on the interacting surface. Under certain operating conditions, these interactions may lead to destruction of vortices in a phenomenon called *vortex breakdown* or *vortex bursting* which may further restrict the performance characteristics of the vehicle. In this article, we present the results of an experimental study involving the head-on interaction of streamwise vortices with

https://doi.org/10.1017/S0022112098001566 Published online by Cambridge University Press

circular cylinders of varying diameters in a Mach 2.49 flow. This investigation was carried out in an attempt to gain insight into aspects of supersonic vortex breakdown observed during previous shock wave/vortex interaction studies. This flow field is particularly suited to such a task because it avoids the large-scale flow unsteadiness observed during previous shock/vortex interaction, while preserving the main features of supersonic vortex breakdown observed during such encounters.

The incompressible aspects of vortex breakdown have been extensively studied over the past 40 years and comprehensive surveys of the subject have been presented in articles, for example, by Benjamin (1962), Sarpkaya (1971), Hall (1972), Leibovich (1984) and most recently by Delery (1994). The vortex breakdown phenomenon is generally characterized by a rapid expansion of the vortex core, formation of stagnation point(s) on the vortex axis, appearance of a reversed flow region, and the presence of large-scale unsteadiness. Low-speed vortex breakdown has been historically observed to take one of two characteristic geometric forms: a bubble-type structure and a spiral-type structure. In addition to this, Sarpkaya (1995) recently reported a conical breakdown in high-Reynolds-number incompressible flows. Experiments performed at supersonic speeds by Zataloka, Ivanyushkin & Nikolayev (1978) and Glotov (1989) had also reported a conical vortex breakdown induced by the imposition of normal shock waves. Furthermore, shock wave/vortex interaction studies reported by Kalkhoran (1994), Smart & Kalkhoran (1995), and Kalkhoran, Smart & Betti (1996) indicated the presence of a conical *vortex distortion*, which possessed many visual characteristics found during low-speed vortex breakdown. However, it is not clear whether the conical vortex breakdown represents a distinct form of vortex breakdown or if it is merely a visual variation of the bubble type.

Whether or not information that has been gathered during studies of low-speed, incompressible vortex breakdown could be extended to high-speed compressible flows is a question of some importance at the present time. With regard to what is meant by the term vortex breakdown at high-speed, it is generally accepted that a vortical structure which exhibits rapid expansion of the vortex core, stagnation point(s) on the vortex axis and a region of reversed flow, may be called a breakdown. Beyond these major defining characteristics however, the similarities between low- and high-speed vortex breakdown may not be very significant. For example, the interplay between a burst vortex core and its surrounding high-speed flow (which will have significant dynamic pressure) may be quite different from its low-speed counterpart. In fact the low-speed spiral type breakdown, which exhibits large non-symmetric lateral fluid movement over a very short streamwise length, is unlikely to have a high-speed counterpart. Furthermore, the fact that any supersonic vortex breakdown must contain a shock wave introduces another important difference between low- and high-speed vortex breakdowns.

Previous studies of supersonic vortex breakdown have been generally devoted to the interaction of streamwise, nearly axisymmetric vortices with otherwise planar normal and oblique shock fronts in a class of problems known as *shock/vortex* interactions. In addition to the practical significance of the shock wave/vortex interactions, these problems are of fundamental importance as they combine many intriguing aspects of fluid dynamic vortices and gasdynamic shock fronts. In these problems, a streamwise vortex is introduced upstream of otherwise planar shock fronts, the planes of which may be either normal or oblique to the vortex axis (figure 1). The structure of the evolving flow field is then dependent upon the strength of the vortex (as determined by flow properties in its core), the intensity of the shock (as dictated by the pressure jump across the shock), and whether the interaction is capable of admitting upstream

https://doi.org/10.1017/S0022112098001566 Published online by Cambridge University Press

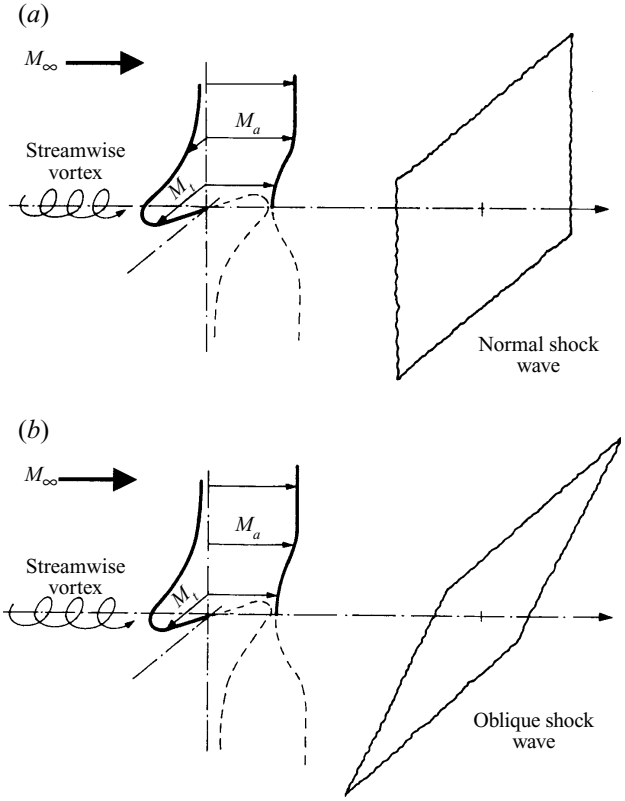


FIGURE 1. Schematic representations of shock wave/vortex interactions: (*a*) normal shock wave, (*b*) oblique shock wave.

propagating disturbances or not. In the light of Benjamin's description (Benjamin 1962) of vortex breakdown, interaction of supersonic vortices with normal shock fronts will always lead to a transition from a supercritical state to a subcritical state. On the other hand, interaction of vortices with oblique shock fronts does not necessarily involve a supercritical to subcritical transition, as supersonic flow is generally preserved downstream of the shock during such encounters. Hence, a key question to be addressed in the study of supersonic vortex breakdown is whether a vortex breakdown resembling that of subsonic flows could occur and, if so, what the parameters governing such situations are. It is quite evident that a supersonic vortex breakdown similar to those observed in subsonic flows must be accompanied by either a strong oblique or a normal shock front to ensure supercritical to subcritical transition.

A supersonic vortex breakdown may be realized by considering the geometry of the interaction between a normal shock and an axisymmetric vortex as shown in figure 1(*a*). In these encounters, the axial velocity of the vortex is reduced from supersonic to subsonic across the shock, while the swirl velocity, being tangent to the shock, will only be marginally affected. For a sufficiently strong shock wave, the vortex may be unable to negotiate such a change while retaining its coherent structure, giving rise to a vortex breakdown. Although the oblique shock interaction shown in figure 1(*b*) contains many of the features present during normal shock encounters, both the axial and swirl velocity components will be significantly affected by the shock, leading to a complicated fully three-dimensional flow field whether or not vortex bursting occurs.

Fundamentally, the shock wave/vortex interaction problems share many charac-

https://doi.org/10.1017/S0022112098001566 Published online by Cambridge University Press

teristic features of the well-documented study involving shock wave/turbulent boundary layer interactions with some exceptions. First, the upstream influence is always present during shock/boundary layer interactions, while as noted above, they may or may not exist during shock/vortex interactions. Secondly, a physically consistent flow model representing shock/boundary layer interaction requires a vanishing velocity at the wall; on the other hand, a viscous wall layer is not needed for interactions involving streamwise vortices which have supersonic velocities on their axis. Nevertheless, it is well documented that separation of a turbulent boundary layer due to shock wave/boundary layer interaction is composed of a stagnation point followed by a recirculating region; these features are also observed during vortex breakdown.

The first published study of shock wave/vortex interaction is due to Zatoloka *et al.* (1978). In their work the interaction between a wing-tip vortex and a normal shock in front of a chocked Pitot-type inlet was investigated. The results of their exploratory study indicated that a conical shock forms as a result of the encounter downstream of which a vortex breakdown and a stagnation zone were postulated. Unfortunately, no measurements were made to quantify the strength off the incoming vortex, and although the vortices were reportedly burst, no measurement of flow properties in the burst region was made to substantiate the presence of a stagnant flow or recirculating region. The geometry of the experimental arrangement was also such that the vortex had weakened in crossing an oblique shock before interacting with the main normal shock front, making it difficult to isolate the influence of the normal shock on the interaction.

The first comprehensive study of normal shock wave/vortex interaction is due to Delery *et al.* (1984). In their study a vortex generator wing was placed in the subsonic portion of a supersonic nozzle while a normal shock was created by a chocked Pitot-type inlet placed in the supersonic test section. As a consequence of this vortex generation methodology, the streamwise vortices used in their study had nearly uniform axial Mach number distributions. Although this arrangement avoids the strong disturbances (shock or expansion waves) created by the wing to influence the interactions, the vortices generated by this approach are weak in comparison to those found in practice. In the light of the fact that the flow-field characteristics during the interaction are governed by the Mach number distribution immediately upstream of the shock front, namely that of the vortex core, the results of the aforementioned study are distinct characteristics of interactions involving vortices having uniform axial Mach number distributions. Nevertheless, the strengths of vortices generated with such an arrangement were found to be sufficient to create interactions with vortex breakdown, which was the essential objective of the above study.

In that combined experimental/numerical investigation by Delery *et al.* (1984), LDV and conical probe measurements were reported before and after the shock. These measurements indicated that normal shock wave/vortex interactions involving vortices above a certain strength lead to vortex breakdown characterized by reversed flow at the vortex axis, reduction in the maximum swirl and an increase in the radius of the vortex core. A vortex breakdown limit was developed using the results of these experiments, indicating an inverse relationship between vortex swirl and shock strength at breakdown. Unfortunately, no visualization of the flow was reported to provide evidence of the type of vortex breakdown. The companion numerical study, which solved the axisymmetric Euler equations, produced breakdown limits similar to the experiments, indicating that the onset of vortex breakdown is dominated by inviscid considerations in this instance. In contrast to the success in predicting the breakdown

https://doi.org/10.1017/S0022112098001566 Published online by Cambridge University Press

limit, the Euler simulations were not able to accurately calculate the observed flow structure after breakdown.

Experimental studies on normal shock wave/vortex interaction reported by Metwally, Settles & Horstman (1989) and Cattafesta & Settles (1992) used wake-like streamwise vortices generated by swirl vanes. The results of their study indicated a weak interaction characterized by a bulged forward shock with a characteristic size on the order of the incoming vortex core diameter; and a strong interaction consisting of a much larger bulged forward shock structure which oscillated at high frequency. Based on extensive schlieren observations of the strong normal shock wave/vortex interactions, a hypothetical physical flow model was reported to partially explain the observed flow features. This hypothetical model was based on two key assumptions: the existence of a stagnation point just downstream of a *bubble shock* and the presence of a recirculating zone. The results of experimental studies of Metwally *et al*. (1989) and Cattafesta & Settles (1992) further extended the vortex breakdown curve of Delery *et al*. (1984) to cover a wider range of free-stream Mach numbers.

The interaction of supersonic wing-tip vortices having wake-like axial Mach number distributions with normal shock waves generated in front of a chocked Pitot-type inlet was investigated by Kalkhoran *et al*. (1996) at Mach 2.49. The experiments indicated that interactions involving moderate and strong vortices lead to the formation of an unsteady conical shock wave with apex well upstream of the inlet. The flow field behind the conical shock was observed to contain two distinct zones: an interior subsonic zone containing fluid from the vortex viscous core, and a surrounding supersonic zone. The high-frequency streamwise oscillations, which this flow structure exhibited, were of the order of the size of the shock-generating inlet. As the presence of stagnation points and a recirculating region could not be conclusively measured in this flow field, the term *vortex distortion* was used in this study to describe the state of the vortex downstream of the conical shock.

It is important to note that the above-mentioned observations were found to be unique features of streamwise vortices exhibiting wake-like axial Mach number distributions and are not necessarily representative of interactions involving uniform or jet-like vortices. Previous supersonic vortex interactions have included both uniform (Delery *et al*. 1984) and wake-like distributions (Metwally *et al*. 1989; Cattafesta & Settles 1992; Smart & Kalkhoran 1995 and Kalkhoran *et al*. 1996), while supersonic vortices possessing jet-like axial Mach number distributions have not been experimentally observed. For streamwise vortices having uniform Mach number distributions, numerical simulations of oblique shock/vortex interactions reported in Rizzetta (1995) and the experimental study of normal shock/vortex interactions in Delery *et al*. (1984) did not indicate vortex distortions similar in shape to those of Smart & Kalkhoran (1995) and Kalkhoran *et al*. (1996) for oblique and normal shock interactions, respectively. The natural conclusion drawn from these observations is the greater role of the vortex-core axial Mach number distribution than previously anticipated during all supersonic vortical interactions. In addition to the above-mentioned studies, numerical simulations of the normal shock wave/vortex interactions have been reported by Kandil & Kandil (1991) and more recently by Erlebacher, Hussaini & Shu (1997). Numerical studies of the oblique shock wave/vortex interactions include the works of Corpening & Anderson (1989), Nedungadi & Lewis (1996), and Rizzetta (1997). Theoretical investigations reported by Mahesh (1996) and Smart & Kalkhoran (1997) have focused on the development of simple techniques to successfully predict vortex breakdown limits during the interaction of streamwise vortices with normal shock fronts.

https://doi.org/10.1017/S0022112098001566 Published online by Cambridge University Press

All the aforementioned experimental studies of normal shock wave/vortex interaction supplied some previously unknown information concerning the behaviour of vortices in supersonic flow. These investigations revealed both bubble (as reported by Metwally *et al*. 1989 and Cattafesta & Settles 1992) and conical (as observed by Zataloka *et al*. 1978 and Kalkhoran *et al*. 1996) disturbances. Unfortunately, only the study of Delery *et al*. (1984) contained measurements of reversed flow downstream of the shock wave, thereby obtaining conclusive proof of supersonic vortex breakdown for vortices having uniform axial Mach number distributions. The major reason for this dearth of quantitative flow measurements has been the large-scale, high-frequency oscillations of the shock structure exhibited by these flows. In the light of this fact, an examination of different shock-generating methods has indicated that an experimental configuration which significantly reduces the large-scale unsteadiness associated with shock/vortex interactions is that of the head-on interaction of a streamwise vortex with a circular cylinder. As will be shown later in this article, the vortex/cylinder interaction experiments of the present study lead to a supersonic vortex breakdown which is *globally* steady; i.e. the flow field is turbulent with its usual time-dependent fluctuations but, it does not exhibit the large-scale oscillations that have hindered measurements in previous shock/vortex interactions. This particular characteristic of the vortex/cylinder interactions is one of the main reasons for studying this very interesting flow field.

The main objective of the present investigation was to experimentally examine the largely unexplored phenomenon of supersonic vortex breakdown. The globally steady supersonic vortex breakdown generated by the head-on interaction of a streamwise vortex with a circular cylinder was the flow field chosen for this task. In particular, both surface pressure measurements on the cylinder, and Pitot-static pressure measurements in the flow were used in conjunction with optical shadowgraph and surface oil flow visualizations to examine the dependence of the burst structure on the incoming vortex strength and the cylinder diameter. This examination supplied important information regarding the parameters that govern the scale and the structure of supersonic vortex breakdown. The results have also enabled a connection to be made between the supersonic vortex breakdown observed in the current study and the vortex distortions previously observed during normal shock wave/vortex interactions.

2. Facility, experimental approach, and instrumentation

The current study of vortex/cylinder interaction was carried out in a 38.1×38.1 cm supersonic blow-down wind tunnel at a nominal test section Mach number of 2.49. The stagnation pressure and temperature for these experiments were 0.45 MPa and 290 K respectively, resulting in a unit Reynolds number of 4.3×10^7 m^{-1}. The duration of a typical wind tunnel run was 3 s, with acquisition of experimental data during the final 2 s. A generic illustration of the experimental arrangement is shown in figure 2. All the interaction experiments utilized a vortex generator consisting of a rectangular half-wing with diamond-shape airfoil section (8° half-angle), a chord length of 50.8 mm, a span of 165.1 mm, and angle of attack capability in the range of 0–10.4°. Vortices of different intensity could be generated by placing the half-wing at various angles of attack. The present investigation utilized three different vortex strengths generated by placing the half-wing at 2.5° (weak), 5.7° (moderate), and 10.4° (strong) angles of incidence.

Two circular cylinders with diameters of 12.7 mm and 25.4 mm were alternately mounted in the test section ceiling 140.5 mm downstream of the vortex trailing edge

https://doi.org/10.1017/S0022112098001566 Published online by Cambridge University Press

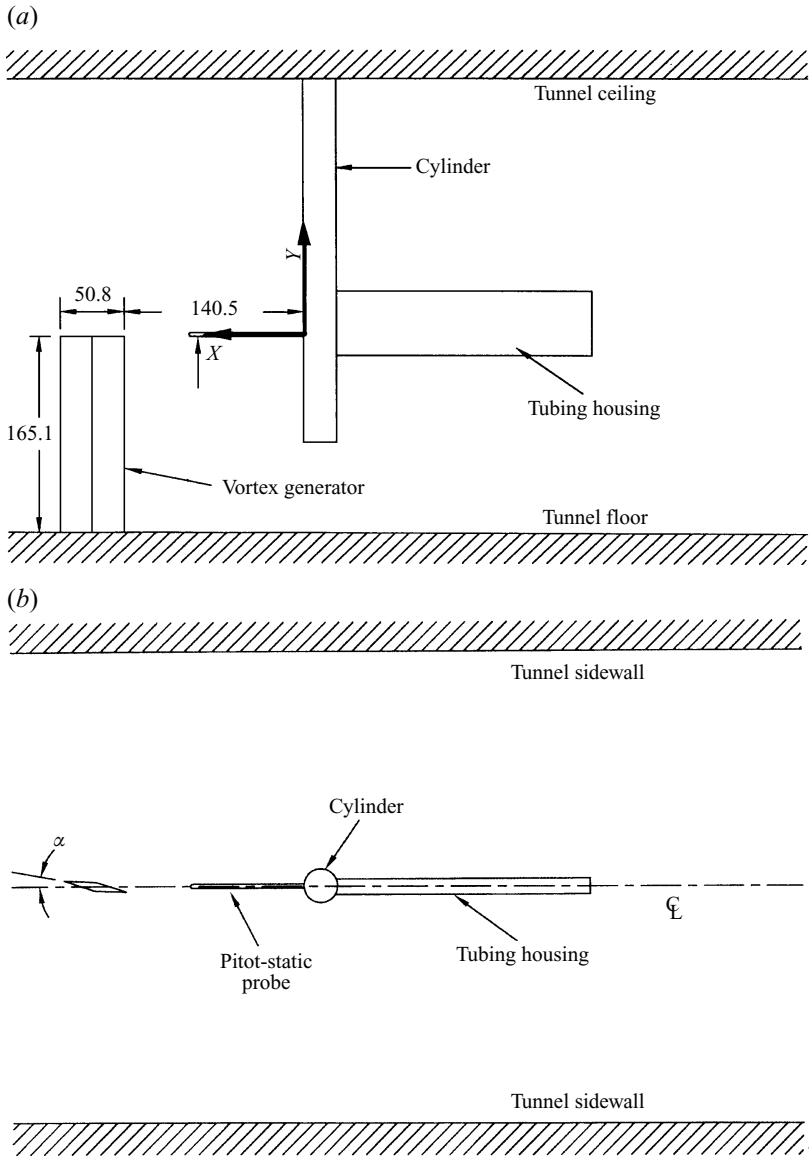


FIGURE 2. Schematic of the experimental arrangement: (*a*) side view, (*b*) top view. All dimensions are in mm.

(figure 2). In the present study, the half-wing and the cylinders were placed at the test section centreline. The positions of the centres of vortices where the Pitot pressures in the vortex cores are minimum, were determined in previous studies (Smart, Kalkhoran & Bentson 1995 and Paek 1997). The downwash of the vortex (measured in the *Z*-direction) was defined as the perpendicular distance from the streamwise plane through the centroid of the half-wing planform to the position of minimum Pitot pressure. The downwashes were measured to be 1.5, 2 and 2.5 mm for the weak, moderate, and strong vortices respectively. As a result of the present experimental arrangement, the vortices strike the cylinders at most 2.5 mm from their respective centrelines. Given the relative size of the cylinders with respect to the downwash distances of the vortices, it is reasonable to assume that the resulting vortex/cylinder interactions represent a

https://doi.org/10.1017/S0022112098001566 Published online by Cambridge University Press

head-on encounter. The larger cylinder was instrumented with a miniature high-frequency pressure transducer (Kulite Model XCQ-062-50A) flush-mounted at the leading edge to detect the anticipated pressure fluctuations in the flow field. The measurement port was verified by shadowgraph flow visualization to be adjacent to the position of vortex impingement on the cylinder. The pressure transducer had an outer diameter of 1.6 mm, a useful range of 0–345 kPa, and a natural frequency response of 60 kHz. The amplified output from the transducer was digitized using a LeCroy 12-bit A/D converter at rates up to 30 kHz.

A United Sensor Model PAC-8-KL Pitot-static probe with eight equally spaced static orifices was used for measurement of the interaction flow field upstream of the cylinder. The probe had a diameter of 3.2 mm and the capability of being traversed in the streamwise direction a distance 91 mm upstream of the cylinder, while the entire cylinder–probe assembly could be moved up or down making it possible to conduct measurements at different vertical locations (figure 2). A conventional uncertainty analysis of the Pitot-static pressure measurements indicated nominal maximum uncertainty values of 0.0041 for both the non-dimensional Pitot (p_t/p_{t_∞}) and static (p/p_{t_∞}) pressures. These uncertainty values include the errors associated with the pressure transducers (linearity and hysteresis), amplifiers, and A/D converters. Experimental evidence to be presented later indicated that for interaction experiments leading to vortex breakdown, the flow field is largely unaffected by introduction of the probe inside the burst region. Accurate conversion of the Pitot-static pressure measurements to a velocity magnitude depends on the applicability of the probe calibration curves to the measurement environment. Measurements taken on the centreline of the expanding vortex core, where the magnitude of swirl velocity is negligible, will supply an accurate measure of any positive axial velocity and also indicate if the axial velocity becomes negative. Away from the centreline, cross-flow velocity components may increase to the point where the angle of attack of the probe is outside the range of its accuracy. As a consequence of this, Pitot-static measurements away from the centreline of the expanding vortex core only supply qualitative information about the local velocity levels.

Optical visualizations of the interaction flow fields were performed using a shadowgraph technique. The shadowgraph system consists of a parabolic mirror with a focal length of 3.7 m and a spark light source which provided microsecond range exposure times. The recording device for the shadow-photographs was a 35 mm camera equipped with a motor drive which provided multiple images of the flow field at a rate of two per second. The camera was loaded with Kodak T-Max™ ASA 3200 film, but was processed as ASA 6400 in Kodak T-Max™ developer to provide a more clear image of the interaction. The shadowgraphs of the flow field taken using this arrangement are quite effective in providing both qualitative and quantitative information about the vortex/cylinder interaction flow structure. Surface flow visualizations were performed on the Pitot-static probe using a mixture of kerosene and lampblack, in order to gain further evidence of reversed flow in the burst region of the vortex/cylinder flow field. These patterns were recorded by motion pictures during a typical wind tunnel run.

3. Characteristics of supersonic wing-tip vortices

A conventional dimensional analysis of the vortex/surface interaction problem indicates that the governing simulation parameters are the free-stream Mach number (M_∞), Reynolds number based on the surface characteristic length, and a vortex

https://doi.org/10.1017/S0022112098001566 Published online by Cambridge University Press

intensity parameter such as the maximum swirl ratio defined as $\tau_{max} = (M_{sw}/M_{ax})_{max}$ where M_{sw} and M_{ax} represent the swirl and axial Mach numbers respectively. A feature of all supersonic vortical interaction problems is that they involve shock fronts for which the jumps in vortex properties are governed by the distribution of Mach number and total pressure within the vortices. Thus, in addition to the above-mentioned parameters, a number of additional vortex related parameters are required to characterize such interactions, namely the axial Mach number at the vortex centreline, M_{axc}, and the normalized total pressure at the vortex centreline, $p_{tc}/p_{t\infty}$. Similar to the shock wave/vortex interaction experiments of Smart & Kalkhoran (1995) and Kalkhoran *et al.* (1996), the present investigation utilized wing-tip vortices exhibiting wake-like axial Mach number distributions.

The flow properties in the core region of the moderate and strong wing-tip vortices were measured using four-hole and five-hole conical probes, as presented in Smart *et al.* (1995). Similar measurements for the weak vortex were made by Paek (1997). These measurements were performed a distance of 113 mm (2.25 vortex generator chords) downstream of the vortex generator trailing edge, i.e. approximately 27 mm upstream of the cylinder leading edge in the current experimental arrangement. The results indicated a significant deficit in the axial Mach numbers and total pressures along with Burgers-like swirl distributions in the vortex cores. Figures 3(*a*) and 3(*b*) illustrate the axial and swirl components of the Mach number respectively. It should be noted that multi-hole conical probes provide direct measurements of local Mach number distributions in the vortex cores but not the velocity field. Evaluation of the velocity field requires knowledge of the sound speed distribution in the vortex, which in turn dictates independent measurements of temperature profiles. The maximum uncertainty values in the measured axial and swirl Mach numbers are on the order of 0.064 and 0.014, respectively. These measurements indicated tightly wound vortices with viscous core diameters of approximately 3.5 mm, 4 mm, and 5.5 mm for the weak, moderate and strong vortices, respectively. As seen in figure 3(*a*), the axial Mach number distributions indicate minimum Mach numbers of 2.1, 1.77 and 1.64 on the axis of respective vortices. Of particular importance to the analysis of the present study is the significant axial Mach number deficit in the wake region of the weak vortex. As evident from figure 3(*a*), unlike the moderate and strong vortices, the weak vortex has a minimum axial Mach number of 1.85 in the wake of a sensible distance below the vortex axis. Due to the non-symmetric swirl profiles, the maximum swirl ratio is calculated for each vortex by averaging the peak values occurring inboard and outboard of the vortex generator, resulting in values of $\tau_{max} = 0.07$, 0.18 and 0.32 for the weak, moderate, and strong vortices, respectively. These measurements further indicated tightly wound vortices with viscous core diameters of approximately 3.5 mm, 4 mm and 5.5 mm for the weak, moderate and strong vortices respectively.

Figure 3(*c*) illustrates the total pressure distributions in the core region of the wing-tip vortices where the maximum uncertainty in the measurements of P_t/P_{t0} are ± 0.025. The generated vortices are seen to be regions of sensible total pressure deficit where for the weak vortex on its axis the minimum total pressure, P_t/P_{t0}, is 0.57. This rather large total pressure drop from the free-stream value to the vortex centre is entirely due to viscous dissipation. Comparatively, on the axis of the moderate and strong vortices, the total pressure losses are seen to be 79% and 88% of their respective free-stream values. It should be noted that Metwally & Settles (1988) also reported total pressure deficits of comparable magnitudes. Such large total pressure deficits in the core of the wing-tip vortices are expected to play a significant role in the study of supersonic vortex interaction problems as they lead to significant entropy gradients upstream of the

https://doi.org/10.1017/S0022112098001566 Published online by Cambridge University Press

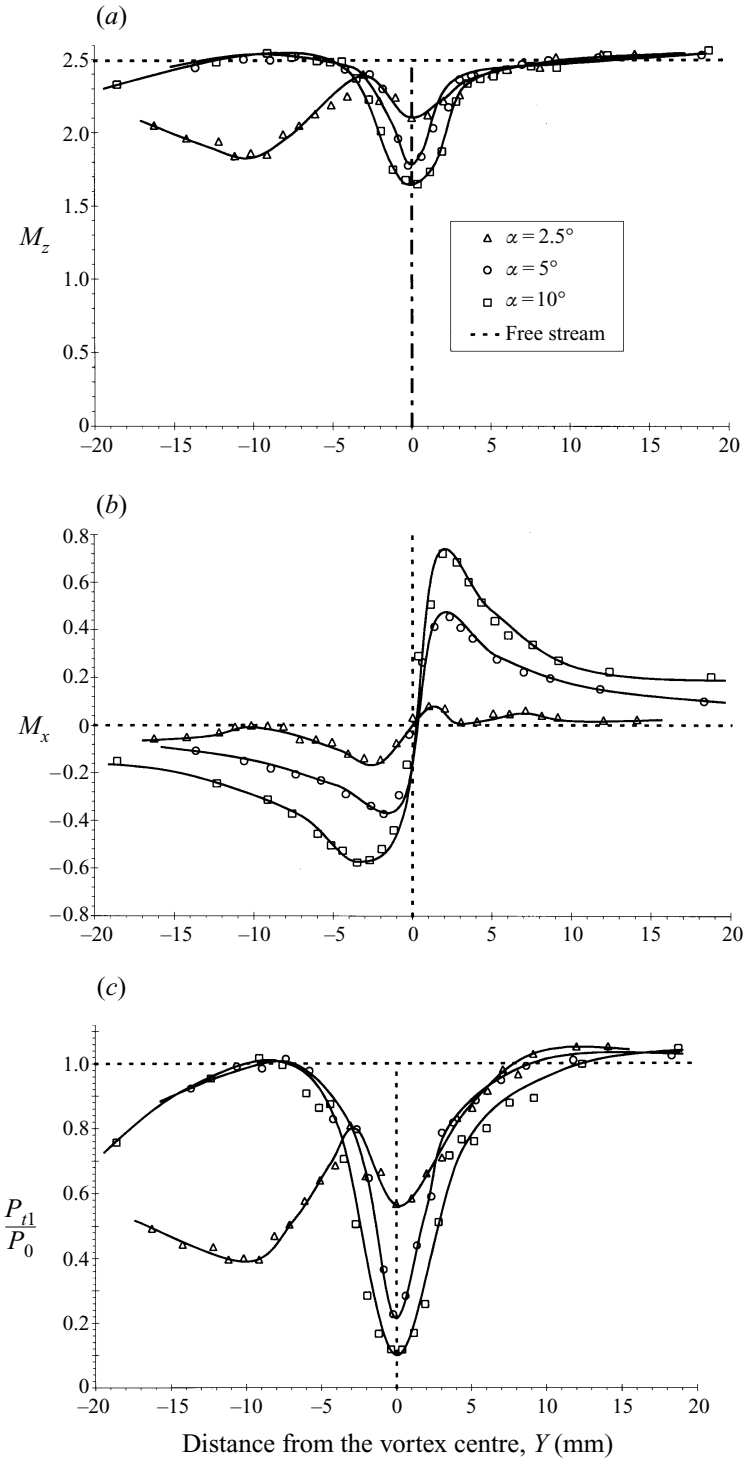


FIGURE 3. Distribution of (*a*) the axial Mach number, (*b*) the swirl Mach number, and (*c*) the total pressure, in the vortex cores.

https://doi.org/10.1017/S0022112098001566 Published online by Cambridge University Press

	Weak vortex	Moderate vortex	Strong vortex
Centreline static pressure, $p_c/p_{t\infty}$	0.062	0.041	0.024
Centreline total pressure, $p_{tc}/p_{t\infty}$	0.567	0.226	0.117
Centreline axial Mach no., M_{axc}	2.10	1.77	1.65
Maximum swirl ratio, τ_{max}	0.07	0.18	0.32

TABLE 1. Flow properties in the vortex cores

shock fronts. This is also of notable importance when theoretical and numerical solution of the problem using an isentropic model for the streamwise vortices is sought. Table 1 summarizes the values of pertinent parameters that characterize the streamwise vortices used for the current vortex/cylinder interaction studies.

4. Experimental results and discussion

4.1. *Weak-vortex interactions*

A shadowgraph image of the flow field containing the larger cylinder in the absence of vortical structure is shown in figure 4. Flow is from left to right (as it is in all the shadowgraphs presented in this article) and the image of this baseline flow depicts a classic bow shock standing upstream of the cylinder. As previously noted, the weak vortex is characterized by $\tau_{max} = 0.07$, $M_{axc} = 2.10$ and $p_{tc}/p_{t\infty} = 0.567$. Figure 5 shows an image of the flow field generated by the head-on interaction of the weak vortex with the cylinder where the vortex-generating half-wing can be seen at the left of the picture. Comparison of figures 4 and 5 clearly illustrates an upstream bulging of the bow shock in response to the addition of the weak vortex generator. The upper limit of this region of upstream shock displacement corresponds approximately with the height of the vortex generator tip. It is unfortunate that the weak vortex (unlike the moderate and strong vortices) cannot be seen in the shadowgraph images. However, from the conical probe measurements it is known that the core of the weak vortex exhibits minimal in-wash, and therefore, must encounter the bow shock close to the point where it begins to deform. The observed bulging of the bow shock must therefore be caused not only by the weak vortex core, but also by the vortex-generator wake. This fact is evident by considering the axial Mach number distribution of the weak vortex as shown in figure 3(*a*) where the wake has a minimum Mach number of 1.85 a distance of 10 mm below the vortex centre. As expected, the point of minimum axial Mach number in the wake corresponds closely with the most upstream location of the bulged-forward shock structure. While the vortex/cylinder interaction flow field depicted in figure 5 contains some evidence of increased turbulence levels downstream of the bulged shock (as compared to downstream of the undisturbed bow shock in the baseline flow), there is no indication that the interaction involving the weak vortex leads to a vortex breakdown. It is also noted that numerous shadowgraph images taken at 0.5 s intervals indicated no evidence of large-scale flow-field unsteadiness, hence the interaction involving the weak vortex was observed to be globally steady.

Time history plots of the surface pressure measured at the leading edge of the cylinder during both the baseline and weak-vortex interaction flows are shown in figure 6, along with the theoretical Pitot pressure behind a normal shock at Mach 2.49. The baseline measurements indicate small-scale fluctuations about a mean level that is slightly above the theoretical Pitot pressure. The measurements involving the weak vortex show a mean level approximately 10 % below the theoretical Pitot pressure and

https://doi.org/10.1017/S0022112098001566 Published online by Cambridge University Press



FIGURE 4. Shadowgraph of the baseline flow field at Mach 2.49.

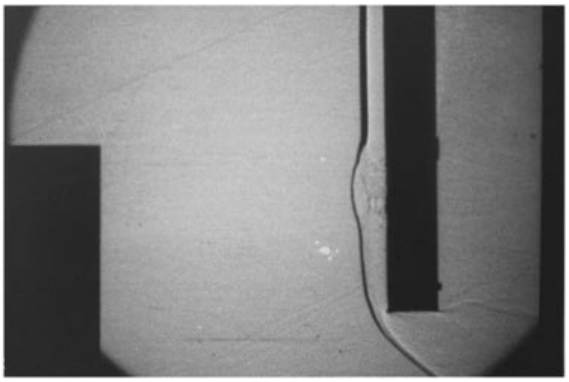


FIGURE 5. Shadowgraph of the flow field during the weak-vortex/cylinder interaction.

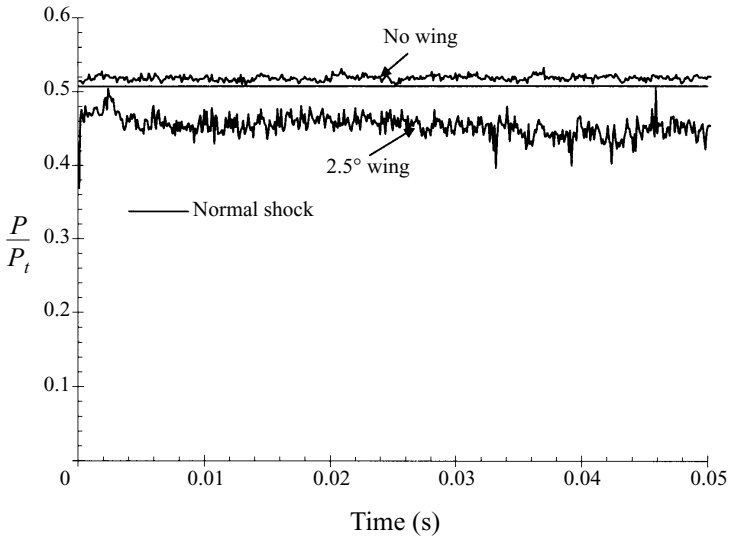


FIGURE 6. Time history of the cylinder leading-edge pressure during the weak-vortex/cylinder interaction.

https://doi.org/10.1017/S0022112098001566 Published online by Cambridge University Press

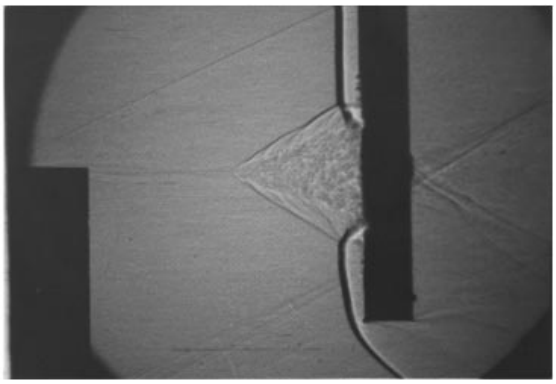


FIGURE 7. Shadowgraph of the flow field during the moderate-vortex/cylinder interaction.

RMS pressure fluctuations of approximately 4% of the mean. The source of the increased pressure fluctuation levels is expected to be the increased turbulence levels in the vortex/wake as compared to the free-stream flow. The differences between the free-stream and the weak-vortex/wake turbulence levels are particularly evident in these surface pressure measurements because of turbulence amplification behind the bow shock. As already noted, further evidence of increased turbulence levels in the weak-vortex interaction can be seen when comparing figures 4 and 5.

4.2. *Moderate-vortex interactions*

Interactions involving the moderate vortex were examined using streamwise wing-tip vortices generated by placing the wing section at 5.7° angle of attack. As shown in table 1, the moderate vortex is characterized by $\tau_{max} = 0.18$, $M_{axc} = 1.77$ and $p_{tc}/p_{t\infty} = 0.226$. This vortex was the weaker of the two considered during the oblique shock wave/vortex interaction experiments of Smart & Kalkhoran (1995) and the normal shock wave/vortex interactions of Kalkhoran *et al.* (1996). In the above studies, the interaction of this moderate vortex with the oblique shock generated by a 29° wedge at Mach 2.49 (i.e. the strongest attached oblique shock wave) did not reveal any significant alteration to either the vortex or the shock wave. On the other hand, interaction with an otherwise normal shock at Mach 2.49 led to a dramatic reorganization of both the shock and the vortex.

Figure 7 shows a shadowgraph image of the moderate-vortex interaction flow field. The image clearly indicates a concentrated streamwise vortex convecting downstream from the half-wing tip and encountering a blunt-nosed conical shock front which is close to a normal shock in the neighbourhood of the vortex core. The apex of the conical shock is seen to be situated approximately 68 mm (2.7 cylinder diameters) ahead of the cylinder, which is a significant distance upstream of the undisturbed shock stand-off shown in figure 4. Furthermore, the vortex core can be seen to expand rapidly downstream of the nearly normal apex of the shock front to form a turbulent conical structure. The oblique portion of the conical shock, which surrounds this turbulent structure, may be perceived to be a response of the outer supersonic flow to the presence of the expanding vortex core. Similar to the familiar case of supersonic flow over a blunt-nosed cone, the flow field is composed of two zones having distinct *entropy* distributions: a subsonic internal zone containing the expanding vortex that has been processed by a strong shock, and an outer supersonic zone which has passed through the oblique portion of the conical shock wave. A noteworthy observation concerning

https://doi.org/10.1017/S0022112098001566 Published online by Cambridge University Press

this flow field is the significantly higher entropy jump experienced by the vortex viscous core in crossing the strong portion of the conical shock wave in comparison to that outside the viscous core where the shock is inclined and significantly weaker.

An interesting feature of the moderate-vortex interaction flow field is the appearance of a thin *shear layer* at the boundary between the two flow regions. This layer is clearly seen in figure 7 just downstream of the conical shock apex, and is a region of large Mach number and entropy gradients. In particular, the fluid velocity continuously varies from subsonic to supersonic Mach numbers across this thin shear layer. Weak compression waves emanating from this *entropy-shear* layer may also be seen in figure 7. These waves propagate through the supersonic flow, which surrounds the expanding vortex core, and meld with the surrounding conical shock. Further downstream, the conical shock meets the cylinder bow shock on either side of the expanding vortex core, creating a typical shock/shock interference pattern. Of practical significance is the serious local heating, and frictional effects that may be experienced by the interacting surface due to such an interference. The bow shock can be seen to curve downstream after encountering the conical shock and terminates at the entropy-shear layer. Additional shock waves can also be seen downstream of the cylinder, suggesting an expansion of the flow behind the cylinder and a subsequent re-compression towards the free-stream direction.

A useful tool for characterizing this and other vortex/cylinder interactions considered in the present study is the concept of an *equivalent cone*. As noted earlier, the oblique portion of the conical shock may be viewed as a response of the free-stream supersonic flow to the expanding vortex core. If the half-angle of an equivalent cone is chosen to be equal to the angle of the entropy-shear layer (measured to be approximately 20° in the moderate-vortex interaction), then the inviscid conical shock wave for this equivalent cone is 32.5°. This corresponds quite closely with the conical shock angle measured in figure 7 to be 32°. This close correspondence suggests that the moderate-vortex/cylinder interaction contains a vortex core which responds to the passage through a nearly normal shock by expanding into a conical form, and a blunt-nosed conical shock which instigates the vortex expansion at its apex. The conical shock then rapidly weakens to an angle which matches the expansion of the vortex core. Such a characterization is further substantiated by considering the fact that upstream of the detached shock wave, the flow field is composed of a rotational region within the vortex viscous core where the gradients of flow properties are large, and an irrotational nearly uniform flow with scale much larger than that of the vortex core diameter. Thus, it is reasonable to expect that the main features of the flow leading to the formation of conical shock wave will be largely governed by the irrotational free-stream flow approaching the equivalent cone surface. The non-uniform Mach number distribution in the vortex core only influences the leading portion of the shock wave creating a curved shock while, outside the vortex core, the shock wave asymptotically weakens to a conical shock structure corresponding to the theoretical shock strength. On the other hand, the geometry of the conical inner region, which is responsible for the formation of the conical shock, depends largely on the vortex-core flow parameters.

The moderate-vortex/cylinder interaction shown in figure 7 is seen to have a striking resemblance to the vortex distortion patterns observed during the normal shock wave/vortex interaction experiments of Kalkhoran *et al.* (1996) with one notable exception, namely the present study resulted in a relatively steady flow field. This important feature of the vortex/cylinder interaction was clearly shown by almost identical shadowgraph images taken at 0.5 s intervals during typical runs. Conversely, the normal shock wave/vortex interactions were observed to be inherently unsteady

https://doi.org/10.1017/S0022112098001566 Published online by Cambridge University Press

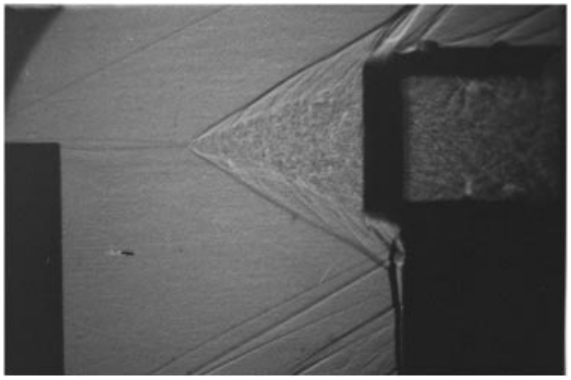


FIGURE 8. Instantaneous shadowgraph of the flow field during moderate-vortex/normal shock wave interaction.

	Moderate-vortex/cylinder interaction	Moderate-vortex/normal shock interaction
Equivalent cone half-angle (deg.)	20	19
Measured shock angle (deg.)	32	31
Theoretical shock angle (deg.)	32.5	31.5

TABLE 2. Measured and theoretical equivalent cone and shock angles for the moderate-vortex interactions

with the entire conical shock and distorted vortex structure oscillating over large distances in the axial direction.

To substantiate the similarities between the two encounters, a distinct state of the flow field during a normal shock/vortex interaction involving the moderate vortex is shown in the shadowgraph of figure 8. In these experiments, a planar normal shock was created in front of a Pitot-type inlet by choking the flow through the inlet. The normal shock generator had a square 63.5 mm × 63.5 mm inlet and was placed 152.4 mm, or three vortex-generator chords downstream of the half-wing. Comparison of figures 7 and 8 indicates that the normal shock/vortex interaction exhibits an expansion of the moderate vortex core identical to that observed in the present study, along with an identical blunt-nosed conical shock with apex well upstream of the inlet entrance. The shadowgraph of figure 8 indicates a conical shock with its leading portion located approximately 71 mm upstream of the inlet while as indicated earlier, the apex of the conical shock was about 68 mm upstream of the cylinder during the present study. A summary of the main geometric features of the two flow fields and a comparison between the measured and theoretical conical shock angles for the two encounters are shown in table 2. Of greater quantitative importance is, however, the identical flow properties in the interaction region as determined by the equivalent cone and the associated shock angles for the two encounters. Examination of table 2 clearly demonstrates nearly identical structures in terms of the equivalent cone and shock angles. In the light of the fact that both these flow fields involved the same vortex and exhibit very similar shock patterns, these flows must contain identical properties just downstream of the respective shocks. Thus, analysis of the observed flow structure during the present investigation is therefore expected to shed light on the many

https://doi.org/10.1017/S0022112098001566 Published online by Cambridge University Press

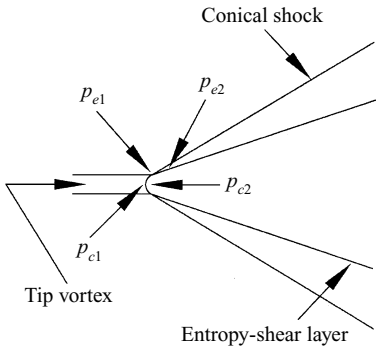


FIGURE 9. Illustration of the pressure jump across the conical shock wave.

unresolved issues concerning vortex distortion patterns observed during previous normal shock/vortex interaction study.

Analysis of the shadowgraphs shown in figures 7 and 8 reveals yet another important aspect of these encounters. The pressure jump imposed upon the vortex at its axis is given by that across a normal shock at Mach 1.77 which has a value of $p_{c2}/p_{c1} = 3.49$. On the other hand, at the outer edge of the vortex, the jump in pressure is given by that across the oblique portion of the conical shock where $p_{e2}/p_{e1} = 1.87$. This trend illustrates a significantly larger amplification of the vortex centreline pressure compared to that at its edge upon crossing the shock. An important consequence of this behaviour is the substantial increase in the ratio of the static pressure on the vortex axis to that at the edge of the vortex (i.e. p_c/p_e) across the shock front. As illustrated in figure 9, upstream of the shock $p_{c1}/p_{e1} = 0.69$ while behind the shock, it sharply rises to a value of $p_{c2}/p_{e2} = 1.29$. This change in the radial pressure gradient from increasing outwards (as typical of an undisturbed vortex) to increasing inwards, must have a significant effect on the vortex and consequently on the structure of the downstream flow. This is a unique feature of the encounters involving supersonic vortex breakdown, which distinguishes the weak- from the moderate-vortex interaction. During the weak-vortex encounter, as evident from the shadowgraph of figure 5, the shock wave remains nearly normal, thus the pressure jump on the vortex centre is approximately the same as that experienced at the outer edge of the vortex, hence $p_{c2}/p_{e2} = p_{c1}/p_{e1}$. Formation of a conical shock has serious consequences when attempting to obtain a theoretical vortex breakdown limit during shock/vortex interactions. It is quite tempting to assume that during such encounters the shock would remain planar and the breakdown will take place downstream of the undisturbed planar normal shock front. However, the results of the present study clearly demonstrate that such an assumption will lead to a significant overestimation of the pressure jump at the outer edge of the vortex.

As stated, the state of the flow field during the normal shock/vortex interaction shown in figure 8 represents an instantaneous snapshot of the flow during a typical run. In contrast, the vortex/cylinder interaction flow field shown in figure 7 is typical of the flow observed throughout an entire run. The only difference between the two flows is their respective downstream boundary conditions. Therefore it must be the downstream boundary condition that introduces the large-scale oscillations exhibited by the normal shock wave/vortex interactions. As a choked Pitot-type inlet was utilized to generate the normal shock in these experiments, the observed unsteadiness is expected to be related to the well-known inlet buzz phenomenon (Newsome 1984), which can produce large-scale flow-field unsteadiness in response to small variations in the mass flow rate through the inlet. This hypothesis suggests that the unsteadiness observed in many

https://doi.org/10.1017/S0022112098001566 Published online by Cambridge University Press

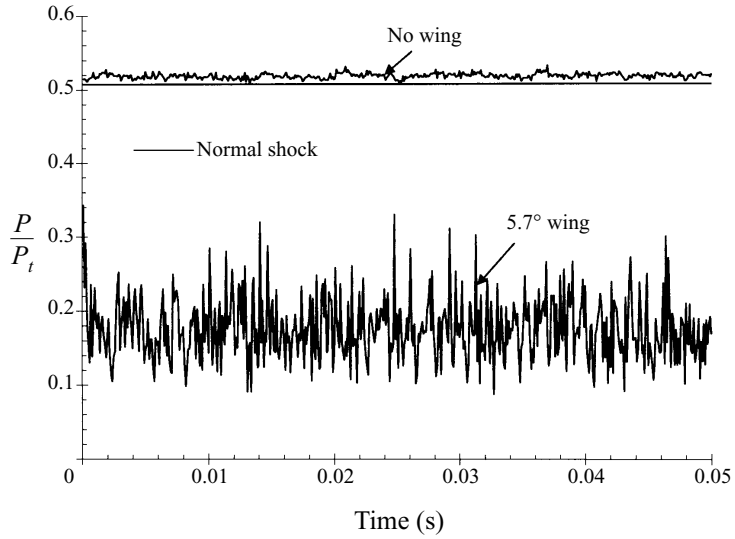


FIGURE 10. Time history of the cylinder leading-edge pressure during the moderate-vortex/cylinder interaction.

previous experiments involving normal shock wave/vortex interactions may not be inherent to the interaction itself, but be dependent on the manner in which the downstream boundary condition is imposed. The vortex/cylinder interaction currently under investigation is essentially a normal shock wave/vortex interaction (the bow shock being normal to the free stream at the cylinder leading edge), but with a different downstream boundary condition than has been previously applied. It is expected that the vortex/cylinder interaction flow field will remain globally steady as long as the cylinder diameter is large compared to the vortex core diameter. This steady behaviour of the resulting flow field makes the geometry of the present interactions more suitable to study supersonic vortex breakdown phenomenon. Alternatively, the normal shock/vortex interaction constitutes a problem of fundamental importance, and a careful arrangement of the experimental methodology may be devised to largely alleviate the observed unsteadiness reported elsewhere.

Measurements of the pressure at the leading edge of the cylinder during moderate-vortex interactions revealed a significant reduction in the magnitude of the measured pressure as shown in figure 10. Moreover, high-amplitude pressure fluctuations about a mean value of approximately $p/p_{t\infty} = 0.17$ are evident. As was shown earlier in figure 3(*c*), the moderate vortex contains a substantial total pressure drop on its axis which, coupled with the total pressure loss across the shock, is largely responsible for such low values of measured pressures on the cylinder surface. Since the generated flow field did not contain large-scale motion of the conical shock wave, in contrast to the Pitot measurements of Kalkhoran *et al.* (1996), they do not contain any large-amplitude pressure fluctuations due to the shock passage. Unlike the normal shock/vortex interactions, examination of the power spectral density distribution did not reveal any dominant frequency content. Thus, the observed large-scale pressure fluctuations are mainly attributed to flow-field fluctuations generated within the interior of the subsonic zone containing the expanding vortex core as well as turbulent fluctuations and their subsequent amplification when the viscous core of the vortex crosses the strong and nearly normal shock front. As will be shown later, this flow structure is a form of supersonic vortex breakdown, and the high-amplitude fluctuations measured on the

https://doi.org/10.1017/S0022112098001566 Published online by Cambridge University Press

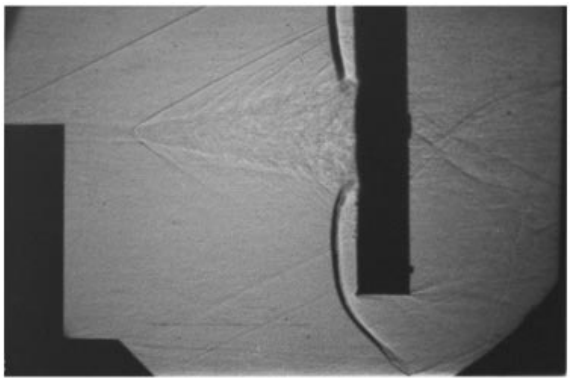


FIGURE 11. Shadowgraph of the flow field during the strong-vortex/cylinder interaction.

cylinder surface are therefore expected to be due to the sensitivity of the recirculating breakdown region to small disturbances.

4.3. *Strong-vortex interactions*

The effect of vortex strength on the evolving flow field was further examined by placing the vortex-generating wing at 10.4° angle of incidence. As previously noted the strong vortex is characterized by $\tau_{max} = 0.32$ (nearly twice the value of the moderate vortex), $M_{axc} = 1.65$ and $p_t/p_{t\infty} = 0.117$. In previous studies, the interaction of this vortex with both the oblique shock wave generated by a 29° wedge and a normal shock at Mach 2.49 led to a significant reorganization of the flow field. Figure 11 shows a shadowgraph image of the flow field generated during a typical strong-vortex/cylinder encounter. Similar to the moderate-vortex interaction case, the vortex may be seen to convect downstream and expand rapidly behind the curved portion of the conical shock to form a turbulent conical region. The leading portion of the conical shock is located approximately 106 mm (4.2 cylinder diameters) upstream of the cylinder which is considerably further upstream than that observed in figure 7 for the interaction involving the moderate vortex. Figure 11 also shows that the resulting flow field is composed of two regions with distinct entropy distributions separated by a relatively organized and distinct boundary in the form of a shear layer. Again, the central turbulent region is composed of fluid particles initially contained within the vortex viscous core, which may be verified by a close examination of the shadowgraph immediately downstream of the leading portion of the conical shock wave.

More detailed comparison between figures 7 and 11 indicates some geometrical differences between the moderate- and strong-vortex interactions. For example, figure 11 shows an equivalent cone half-angle for the interior subsonic region of 14° as compared with 17° for the moderate-vortex interaction. The associated conical shock angle is also less than that of the moderate-vortex interaction, which is measured to be 27.8°. Following the arguments of §4.2, and assuming a Mach 2.49 flow over a 14° half-angle cone, the inviscid theoretical conical shock angle is approximately 28°. Once again there is a remarkable agreement between the measured shock angle and that obtained from supersonic conical flow theory. This result gives further credence to the suggestion that the formation of the conical shock is simply a response of the free-stream supersonic flow to the expanding vortex core. As the only difference between the moderate- and strong-vortex interactions is the character of the vortex, these geometrical differences are necessarily vortex dependent.

A comparison of the strong-vortex interaction flow field with the corresponding

https://doi.org/10.1017/S0022112098001566 Published online by Cambridge University Press

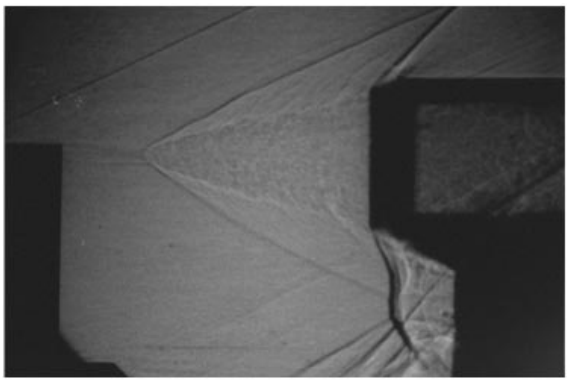


FIGURE 12. Shadowgraph of the flow field during the strong-vortex/normal shock wave interaction.

	Strong-vortex/cylinder interaction	Strong-vortex/normal shock interaction
Equivalent cone half-angle (deg.)	14	13.6
Measured shock angle (deg.)	27.8	27
Theoretical shock angle (deg.)	28	28

TABLE 3. Measured and theoretical equivalent cone and shock angles for strong-vortex interactions

shadowgraph images from the normal shock wave/vortex interaction studies of Kalkhoran *et al.* (1996) also shows remarkable similarities. A typical instantaneous shadowgraph of the strong normal shock wave/vortex interaction flow field is shown in figure 12. In the above picture, the leading portion of the conical shock is seen to be approximately 102 mm upstream of the inlet which compares well with that of the present study. As summarized in table 3, both interactions lead to identical expanding vortex cores and shock geometries. It is also worth emphasizing that this similarity of flow structure occurs despite the fact that the vortex/cylinder configuration contains an enforced stagnation point, whereas the normal shock wave/vortex interaction does not.

Examining figures 11 and 12 as in the previous section, the shock-induced pressure jump at the vortex axis is given by that across a normal shock at Mach 1.65, i.e. a value of $p_{c2}/p_{c1} = 3.01$. At the outer edge of the vortex the jump in pressure is given by that across a 27.8° conical shock at Mach 2.49, i.e. a value of $p_{e2}/p_{e1} = 1.40$. The axis to edge pressure ratios before and after the shock are then $p_{c1}/p_{e1} = 0.40$ and $p_{c2}/p_{e2} = 0.87$ respectively. Note that in contrast to the moderate-vortex interaction, the radial pressure gradient remains increasing outwards after the shock. This fact is consistent with the slower vortex core expansion angle observed for the strong-vortex interaction as compared to the moderate-vortex interaction.

A time history plot of the surface pressure measured at the leading edge of the cylinder during the strong-vortex interaction is shown in figure 13. In a similar fashion to the moderate-vortex interaction, the mean surface pressure of $p/p_{t\infty} = 0.14$ is significantly below the undisturbed level and high-amplitude pressure fluctuations are observed. Again, such low values of the measured pressures are the results of large total pressure deficits in the vortex core (figure 3*c*) and subsequent losses across the strong

https://doi.org/10.1017/S0022112098001566 Published online by Cambridge University Press

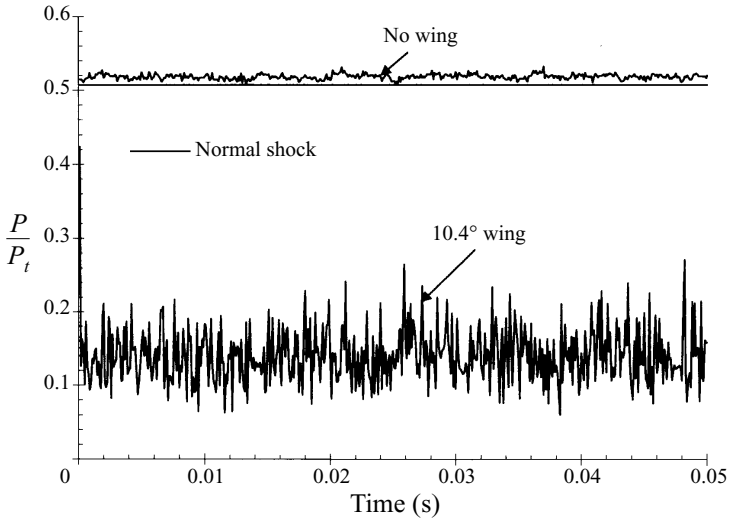


FIGURE 13. Time history of the cylinder leading-edge pressure during the strong-vortex/cylinder interaction.

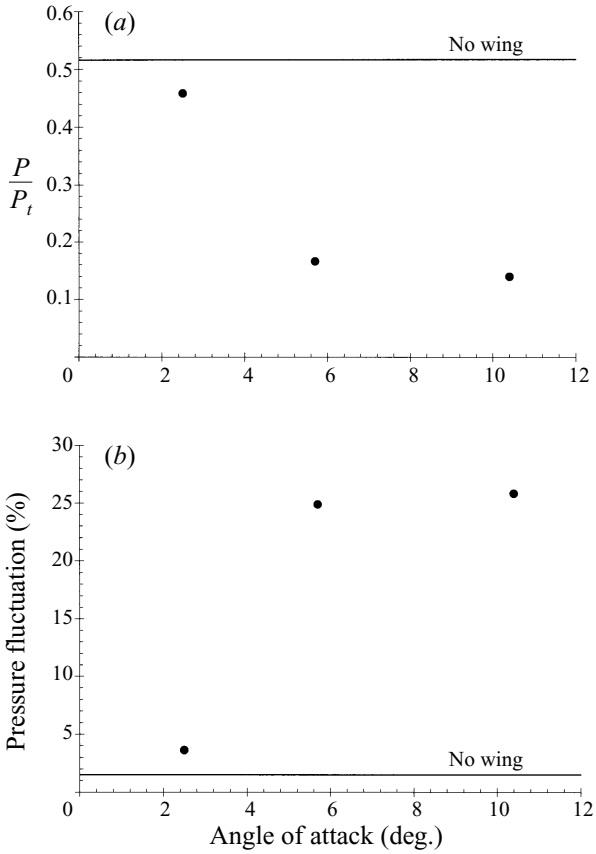


FIGURE 14. Measured (*a*) mean pressures and (*b*) fluctuating pressures at the cylinder leading-edge during strong-vortex/cylinder interaction.

https://doi.org/10.1017/S0022112098001566 Published online by Cambridge University Press

shock front. Similar to the moderate-vortex interaction tests, analysis of the power spectral density did not reveal any dominant frequencies and these fluctuations are once again attributed to the sensitivity of the recirculating breakdown region to small disturbances. The mean and fluctuating pressures measured for all three interactions as well as that of the baseline flow are plotted in figures 14(*a*) and 14(*b*) respectively. These plots show that both the moderate- and strong-vortex interactions generate similar mean and fluctuating pressure levels on the cylinder, values that are quite different from the weak-vortex interaction. These results suggest that the measured pressure on the cylinder is insensitive to vortex strength once vortex breakdown has occurred. On the other hand, it is expected that a rapid change in the mean and fluctuating pressure levels would occur at the minimum vortex-generator angle of attack that leads to vortex breakdown in the current configuration.

5. The effect of downstream boundary condition on the interaction

An important aspect of supersonic vortex interaction problems is whether they are capable of admitting upstream propagating disturbances. The spatial extent of the downstream boundary capable of propagating upstream instabilities is governed by the scale of the subsonic flow behind the normal shock front. In the present study, the influence of the downstream boundary on the flow field was examined by conducting a series of experiments involving interaction of streamwise vortices with a small cylinder of diameter $d = 12.7$ mm, i.e. half the size of the larger cylinder. Figure 15 is a typical spark shadowgraph of the flow generated when the moderate vortex has a head-on encounter with the smaller cylinder. In a similar fashion to the moderate-vortex interactions involving the larger cylinder, a globally steady two-zone flow structure occurs. However, it appears that the size of the structures in the flow field have decreased by the same factor as the cylinder diameter. For instance, the conical shock apex sits 36 mm or 2.8 diameters upstream of the smaller cylinder, as compared with 2.7 cylinder diameters upstream of the larger cylinder. In contrast, the measured equivalent cone half-angle and conical shock angle are almost identical to those measured for the larger cylinder, and therefore show no dependence on the cylinder diameter. The pertinent geometrical angles for the moderate-vortex interaction involving the smaller cylinder are listed in table 4.

Figure 16 shows a shadowgraph image of the flow field generated by the head-on interaction of the strong vortex with the smaller cylinder. Once again the globally steady two-zone flow structure can be seen to scale directly with the cylinder diameter, with the shock apex 55 mm or 4.3 diameters upstream of the cylinder, as compared to 4.2 diameters for the larger cylinder. Table 4 also contains the pertinent geometrical angles for this interaction, indicating almost identical values to the interaction involving the larger cylinder shown in table 3. These observations suggest that in high-Reynolds-number flows, the geometry of the supersonic vortex breakdown generated by a vortex/cylinder interaction depends mainly on the properties of the incoming vortex. Conversely, the scale of the breakdown depends mainly on the size of the cylinder, i.e. the size of the downstream boundary capable of propagating upstream disturbances. Both these results suggest that the scale and geometry of supersonic vortex breakdown is dominated by inviscid phenomena, and that Reynolds number effects are secondary. It must be emphasized, however, that the details of the internal structure of the breakdown region will be dominated by viscous phenomena as this part of the flow field involves the interplay between a recirculating region and a surrounding subsonic flow.

https://doi.org/10.1017/S0022112098001566 Published online by Cambridge University Press

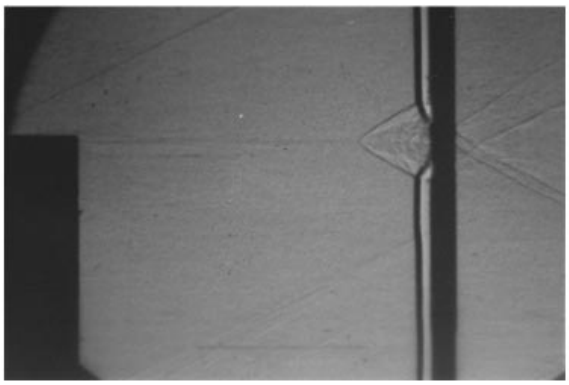


FIGURE 15. Shadowgraph of the flow field during the interaction of a moderate vortex with the small cylinder.

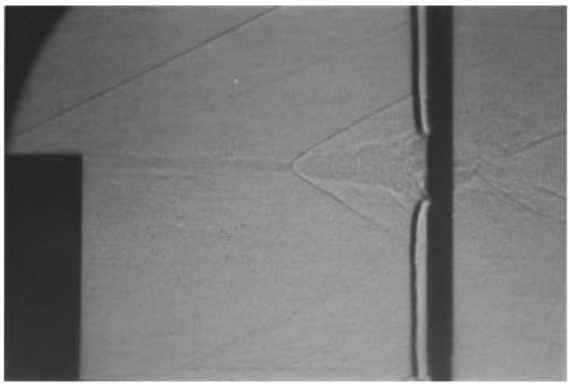


FIGURE 16. Shadowgraph of the flow field during the interaction of a strong vortex with the small cylinder.

	Moderate-vortex/cylinder interaction	Strong-vortex/cylinder interaction
Equivalent cone half-angle (deg.)	20	13
Measured shock angle (deg.)	31.8	28.5
Theoretical shock angle (deg.)	32.5	28

TABLE 4. Measured and theoretical equivalent cone and shock angles for moderate and strong vortices interacting with $d = 2.7$ mm cylinder

6. Vortex distortion vs. supersonic vortex breakdown

The dramatic flow reorganization observed during the vortex/cylinder interactions contains many visual features that suggest it is a form of supersonic vortex breakdown. This flow field also resembles the vortex distortion patterns observed in previous normal shock wave/vortex interaction experiments reported by Kalkhoran *et al.* (1996), the head-on interaction of supersonic vortices with sharp leading edges reported by Kalkhoran (1994), and to some extent the separated shock structure observed during oblique shock wave/vortex interaction experiments of Smart &

https://doi.org/10.1017/S0022112098001566 Published online by Cambridge University Press

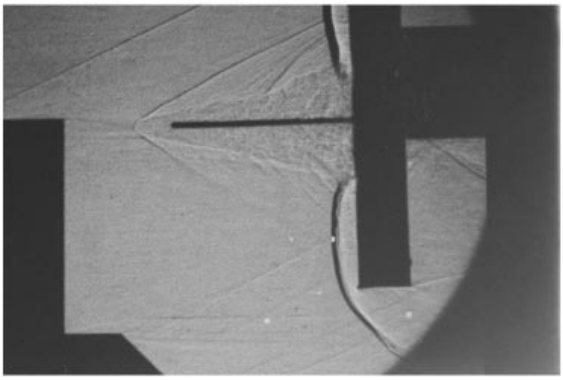


FIGURE 17. Shadowgraph of the flow field during the strong-vortex/cylinder interaction with the Pitot-static probe 91 mm upstream of the large cylinder.

Kalkhoran (1995). In all of these cases, the vortex interaction problem degenerates into that of a streamwise vortex crossing a strong shock front and expanding to form a turbulent conical subsonic region. Irrespective of the type of interaction, distortion of supersonic streamwise vortices occurs at subsonic Mach numbers, thus many characteristics of low-speed vortex breakdown may be expected to be present for supersonic streamwise vortices. Among these characteristics are the formation of stagnation point(s) on the vortex axis and a region of reversed flow. As stated, attempts to definitively measure stagnation points and/or flow recirculation in these previous studies have not been successful. The reasons for these failures have been the large-scale flow-field oscillations observed in the interactions involving normal shock waves and sharp leading edges, and the small size of the conical subsonic region observed in the interactions involving oblique shocks. The current vortex/cylinder configuration supplies a large globally steady flow structure which is adjacent to the cylinder. This flow is ideally suited for conducting the Pitot-static probe measurements needed for definitive proof that the phenomenon previously called vortex distortion is in fact a form of supersonic vortex breakdown.

Pitot-static probe surveys within the conical subsonic zone of the strong-vortex/cylinder interaction involving the larger cylinder were conducted. The probe was centred on the axis of the conical subsonic zone for these measurements and traversed in the streamwise direction. Because the axis of the conical subsonic zone coincides with the axis of the incoming vortex, the swirl velocity component will be negligible in this region. These measurements are therefore expected to provide an accurate measure of any positive axial velocity component, and also indicate if the sign of the axial velocity becomes negative. A shadowgraph image of the probe at its furthest upstream extent (91 mm or 3.6 diameters upstream of the cylinder) is shown in figure 17. Comparison of figure 17 with the shadowgraph taken in the absence of the probe (figure 11) clearly demonstrates that the addition of the probe has no effect on the overall structure of the interaction. The nearly identical shock strengths in the above pictures indicate that the flow properties are quantitatively identical in both flow fields. Shadowgraphs taken with the probe at all measurement positions indicated that this was true for all measurements taken on the axis of the conical subsonic zone. It should be noted that although the introduction of the probe does not alter the state of the flow field during the interactions of the present work involving vortex breakdown, an intrusive device may precipitate vortex breakdown should the vortex be near its critical state.

https://doi.org/10.1017/S0022112098001566 Published online by Cambridge University Press

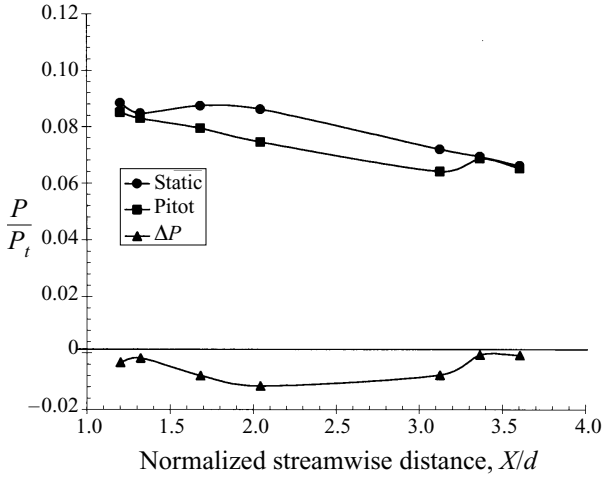


FIGURE 18. Streamwise distribution of the measured pressures during the strong-vortex/cylinder interaction at $Y/d = 0$.

Figure 18 shows plots of the normalized static and Pitot pressures measured between $X/d = 1.2$ and $X/d = 3.6$ (where d is the diameter of the cylinder and $X = 0$ is at the cylinder leading edge) on the axis of the conical subsonic zone. The normalized difference between the Pitot and static pressures is also shown. It is very interesting to note that between $X/d = 1.3$ and $X/d = 3.4$ the static pressure is higher than the Pitot pressure, indicating a region of reversed flow. Furthermore, the Pitot and static pressures were measured to be almost equal at both ends of this region. These measurements suggest the presence of a recirculation region bounded at $X/d = 1.3$ and $X/d = 3.4$ by stagnation points. Independent evidence of the presence of reversed flow was also obtained by introducing a mixture of kerosene and lampblack to the surface of the Pitot-static probe when it was at its most upstream position. Motion pictures of the flow taken during typical wind tunnel runs indicated an upstream displacement of the mixture which could only be caused by a reversed flow within the conical subsonic region. As noted in the Introduction, a high-speed vortex breakdown is generally considered to be a flow which exhibits rapid expansion of the vortex core, stagnation point(s) on the vortex axis and a region of reversed flow. Together with the shadowgraph images presented earlier, these Pitot-static pressure measurements and accompanying motion pictures are considered to supply definitive evidence that the strong-vortex/cylinder interaction leads to a high-speed vortex breakdown, and in particular a supersonic vortex breakdown. Due to its similar flow structure, the moderate-vortex/cylinder interaction must also generate a vortex breakdown. Finally, the nearly identical flow structures observed during normal shock wave/vortex interactions involving the moderate and strong vortices (as compared with the corresponding vortex/cylinder interactions) indicate that the flow structure previously referred to as vortex distortion is indeed a form of supersonic vortex breakdown.

The current results are further substantiated by comparison of the vortex/cylinder interactions with the normal shock wave/vortex interaction breakdown curve of Delery *et al.* (1984) shown in figure 19. On this graph of τ_{max} versus free-stream Mach number, the weak-vortex interaction falls under the breakdown limit (indicating no expectation of breakdown) while the moderate- and strong-vortex interactions fall above the breakdown limit (indicating breakdown is expected). Hence the Pitot-static measurements and shadowgraph images presented in the current study are consistent

https://doi.org/10.1017/S0022112098001566 Published online by Cambridge University Press

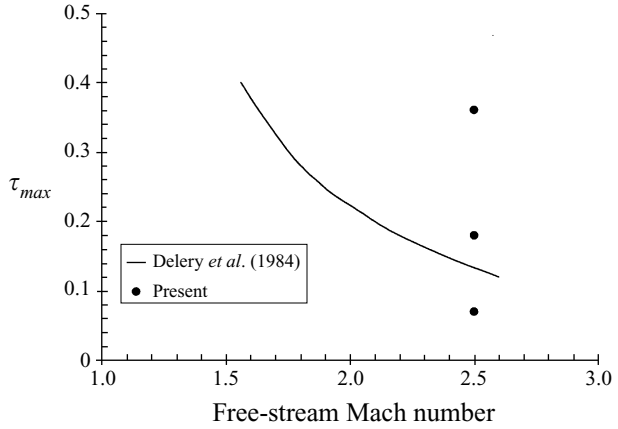


FIGURE 19. Comparison of the supersonic vortex breakdown to the vortex breakdown limit of Delery *et al.* (1984).

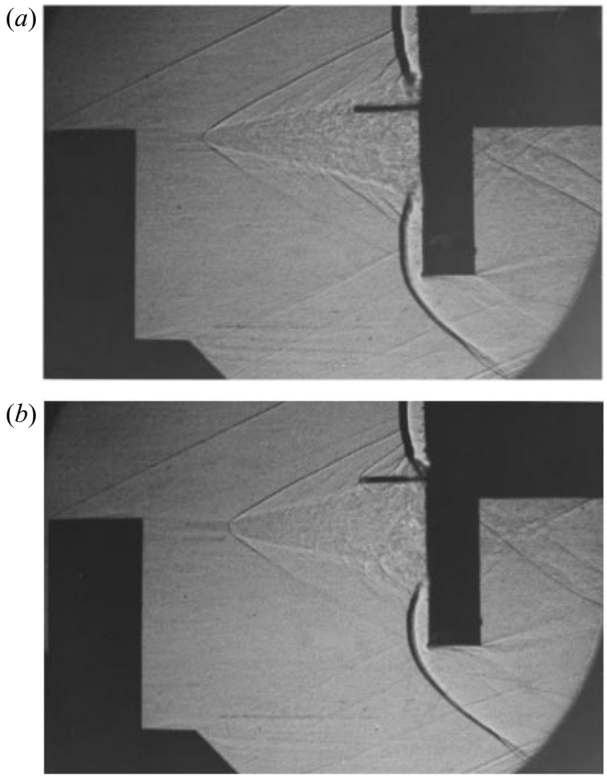


FIGURE 20. Shadowgraph of the flow field during the strong-vortex/cylinder interaction with the Pitot-static probe at (*a*) $Y/d = 0.542$, (*b*) $Y/d = 0.912$.

with predictions of the occurrence of supersonic vortex breakdown based on established breakdown limits.

The strong-vortex interaction flow field was examined further by conducting a vertical Pitot-static probe traverse at $X/d = 1.25$, i.e. slightly downstream of the recirculating region. As previously noted, these measurements only supply qualitative information about the Pitot and static pressure levels in the flow, due to the possibility

https://doi.org/10.1017/S0022112098001566 Published online by Cambridge University Press

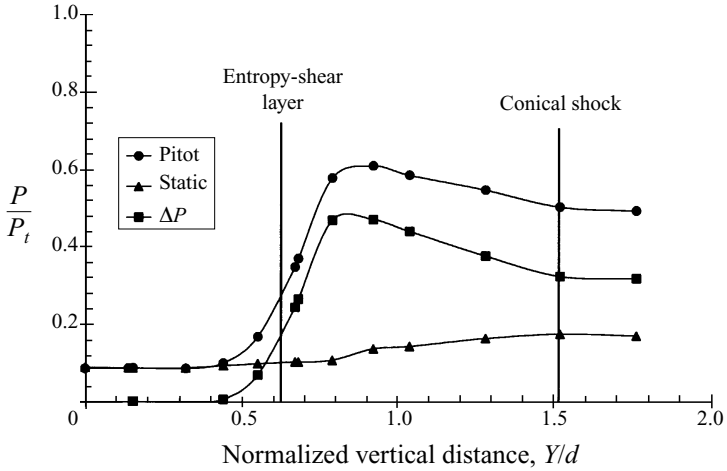


FIGURE 21. Vertical distribution of the measured pressures during the strong-vortex/cylinder interaction at $X/d = 1.25$.

of increased cross-flow velocity components away from the centreline of the conical subsonic zone. Figures 20(*a*) and 20(*b*) show shadowgraph images taken with the probe at $Y/d = 0.542$ and $Y/d = 0.912$ respectively (where $Y = 0$) corresponds with the axis of the conical subsonic zone). Figure 20(*a*) shows an image with the probe tip slightly below the entropy-shear layer, whereas figure 20(*b*) shows an image with the probe tip immersed in the outer supersonic flow (as evident by the shock wave that forms ahead of the probe). Once again, comparison of figures 20(*a*) and 20(*b*) with previous images of the strong-vortex interaction reveal no changes in the overall flow structure attributable to the addition of the probe.

The distributions of Pitot, static and differential pressures measured during the traverse are shown in figure 21. The locations of the shear-entropy layer as well as the conical shock are also shown in the above figure. Interestingly, the Pitot and static pressure levels remain constant and almost identical until just below the entropy-shear layer, indicating low velocity levels within the conical subsonic zone. Once the probe reaches the entropy-shear layer, the Pitot pressure begins to increase significantly, reaching a peak just above the entropy-shear layer before reducing to a level consistent with supersonic flow behind the oblique portion of the conical shock. In contrast, the static pressure remains relatively constant across the entropy-shear layer before increasing slightly once the probe is well into the supersonic flow region. This indicates that while the entropy-shear layer separates two flows with significantly different Mach numbers and total pressures, the static pressures in the two flows are nearly matched across the layer.

Given the information obtained about the vortex/cylinder interaction in the current study, a physical model for the supersonic vortex breakdown flow field observed during the moderate- and strong-vortex/cylinder interactions is shown in figure 22. This model contains a conical recirculation region centred on the axis of the incoming vortex, which is situated within the expanding turbulent zone observed in the shadowgraphs. This recirculation region generates a flow field similar to that which would be produced by a solid conical body protruding upstream of the cylinder. The blunted conical shock observed in the shadowgraphs can therefore be viewed as the bow shock associated with the recirculation zone. As the blunted nose of the shock was observed in all cases to be of the same size as the incoming vortex core diameter, the

https://doi.org/10.1017/S0022112098001566 Published online by Cambridge University Press

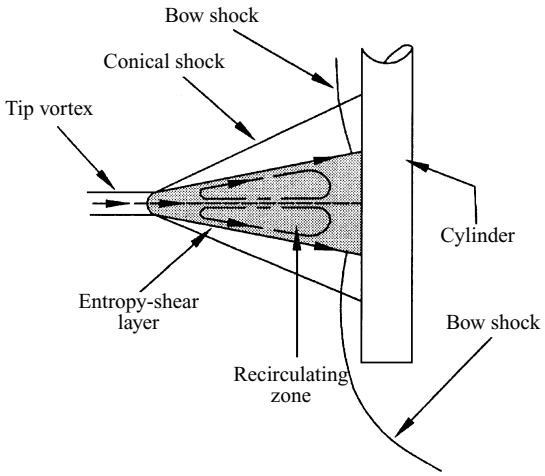


FIGURE 22. Physical model of conical supersonic vortex breakdown.

nose of the recirculation region is expected to be of similar size to the vortex core. To complete the model, the entropy-shear layer is assumed to be a thin constant-static-pressure layer which separates the vortex core fluid, which has been processed by the strong portion of the conical shock, from the outer fluid which passes through the oblique portion of the conical shock. All flow within the entropy-shear layer is subsonic, whereas all flow outside remains supersonic. Close to the cylinder the conical shock forms a shock/shock interference pattern with the cylinder bow shock, which curves downstream and terminates at the entropy-shear layer. A similar physical model is expected to be applicable to the normal shock wave/vortex interactions of Kalkhoran *et al*. (1996), but with the cylinder and its bow shock replaced by a normal shock.

Considering the supersonic vortex breakdown flow model shown in figure 22, it is appropriate to discuss the parameters which are expected to determine the particular geometry of different interactions. As described in previous sections, both the character of the incoming vortex and the size of the cylinder are seen to have an influence on the vortex/cylinder interaction flow fields. Given this, it is interesting to note that the consequences of varying these parameters over the ranges examined in this study appears to be independent, i.e. the physical size of the interaction scales directly with cylinder diameter, whereas the geometry of the interaction appears to be solely dependent on the incoming vortex. While direct scaling of the interaction structure with cylinder diameter suggests that the interaction geometry is determined mainly by inviscid phenomena (i.e. Reynolds number effects are secondary), the particular vortex parameters that are responsible for the different geometries observed for the moderate- and strong-vortex interactions are not known. In terms of M_{axc} and $p_{tc}/p_{t\infty}$, the moderate and strong vortices are fairly similar. However, their respective values of τ_{max} differ by a factor of two. It is not entirely clear however, why a vortex with larger swirl should lead to a supersonic vortex breakdown with smaller equivalent cone angle. Unfortunately the effect of free-stream Mach number on the interaction could not be explored in the current study.

It is also appropriate to make some comparisons between the supersonic vortex breakdown observed in the current study and classical low-speed vortex breakdown. While the supersonic vortex breakdown flow fields presented in the current study contain the major defining characteristics of low-speed vortex breakdown, they do not

https://doi.org/10.1017/S0022112098001566 Published online by Cambridge University Press

exhibit the large-scale unsteadiness typical of many low-speed breakdowns, and the instigating pressure rise occurs in the form of a strong shock wave, as opposed to a gradual pressure rise. A further characteristic that distinguishes supersonic vortex breakdown from established low-speed results is its associated upstream influence. In low-speed flows, vortex breakdown generally occurs in close proximity to the point of application of the adverse pressure gradient. In contrast, the results of the current study indicate that vortex breakdown is initiated well upstream of the undisturbed bow shock. This behaviour is not fully understood at the present time, but it can be categorically stated that it is not due entirely to an increased shock stand-off in response to the Mach number deficit in the vortex cores. The best available analogy for this phenomenon is perhaps the upstream influence observed in separating shock/boundary layer interactions. Despite the aforementioned differences, the current vortex/cylinder interactions that lead to breakdown do show a striking visual resemblance to the incompressible conical vortex breakdown recently observed by Sarpkaya (1995) in high-Reynolds-number turbulent flows. Considering the fact that the current study was conducted at high Reynolds number and that the breakdown occurs in the subsonic flow downstream of a nearly normal shock, such a similarity may not be coincidental.

7. Conclusions

An experimental study of the head-on interaction of streamwise vortices having wake-like axial Mach number distributions with circular cylinders was conducted at Mach 2.49. The main objective of these experiments was to investigate the largely unexplored phenomenon of supersonic vortex breakdown. Unlike previously examined normal shock wave/vortex interaction configurations, the vortex/cylinder interaction generates a globally steady breakdown which is ideally suited for conventional measurements. The results of the present experiments indicated that the geometry of the interaction structure is strongly dependent on the character of the incoming vortex. Shadowgraph images of interactions involving a weak vortex showed some bulging of the cylinder bow shock in response to the vortex and the half-wing wake but no evidence of vortex breakdown. In contrast, interactions involving both moderate and strong vortices were observed to lead to a dramatic reorganization of the flow field which resembled that produced by a conical solid body protruding upstream of the cylinder. These supersonic vortex breakdown flow fields contain a blunt-nosed conical shock with apex far upstream of the undisturbed shock stand-off distance, and vortex cores which pass through the nearly normal apex of the conical shock and expand to form turbulent conical structures. Furthermore, an entropy-shear layer is observed to separate the conically expanding subsonic vortex core from the outer supersonic flow behind the oblique portion of the conical shock. The geometry of these flows could be characterized by an equivalent cone with half-angle equal to the angle of the entropy-shear layer. For both moderate- and strong-vortex interactions, the oblique portion of the conical shock surface is then seen to closely match the theoretical conical shock angle corresponding to the equivalent cone at the free-stream Mach number.

The influence of downstream boundary condition on the interaction structure was investigated by varying the cylinder diameter. Interestingly, decrease of the cylinder diameter by a factor of two decreases the size of the moderate- and strong-vortex interactions by an almost identical factor, but has no discernible effect on the particular interaction geometries, i.e. the equivalent cone and shock angles. These results suggest that the overall size and geometry of supersonic vortex breakdowns observed during

https://doi.org/10.1017/S0022112098001566 Published online by Cambridge University Press

the present study are dominated by inviscid phenomena. Pitot-static probe surveys were conducted inside the expanding vortex core of the strong-vortex interaction. These measurements indicated the presence of a reversed flow on the centreline of the conical subsonic zone, thereby obtaining definitive proof that the flow reorganizations associated with the moderate- and strong-vortex/cylinder interactions are examples of supersonic vortex breakdown. These measurements further indicated that the entropy-shear layer is a constant-pressure interface between an interior flow with low velocity and an outer supersonic flow. Time-dependent pressure measurements were obtained on the cylinder surface adjacent to the position of vortex impingement. These measurements indicate a significant change in the mean and fluctuating pressure levels once the supersonic vortex breakdown structure occurs. The observed large-amplitude pressure fluctuations are attributed to the sensitivity of the recirculating breakdown region to small disturbances and amplification of turbulence levels in crossing the strong shock front.

The moderate- and strong-vortex/cylinder interaction flow fields of the current study are seen to be nearly identical to instantaneous flow structures observed in the highly unsteady vortex distortions generated by normal shock wave/vortex interactions involving the same vortices. This similarity of instantaneously observed flow structure indicates that the phenomenon previously called vortex distortion is a form of supersonic vortex breakdown. Therefore the large-scale unsteadiness observed in previous shock wave/vortex interaction flows may not be inherent to vortex breakdown, but be a consequence of the imposed downstream boundary condition.

A supersonic vortex breakdown model consistent with the results of the current experiments was presented. It contains a conical recirculation region with nose diameter of the same scale as the vortex core diameter, a constant-pressure entropy-shear layer and a blunt-nosed conical shock with apex centred on the incoming vortex. In the light of this physical model, a question of fundamental importance is whether supersonic vortical interactions leading to vortex breakdown can be simulated by modern CFD schemes. The significant upstream influences observed during supersonic vortex breakdown and the mixed subsonic–supersonic zones created as a result of the encounter make the shock/vortex interaction problem a challenging flow field for validating computational techniques.

The assistance provided by Lester Orlick, Alexander Betti, and Ivana Milanovic was greatly appreciated during the experimental study.

REFERENCES

Benjamin, T. B. 1962 Theory of the vortex breakdown phenomenon. *J. Fluid Mech.* **14**, 593–629.

Cattafesta, L. N. & Settles, G. S. 1992 Experiments on shock/vortex interaction. *AIAA Paper* 92-0315.

Corpening, G. & Anderson, J. 1989 Numerical solutions to three-dimensional shock wave/vortex interaction at hypersonic speeds. *AIAA Paper* 89-0674.

Delery, J. M. 1994 Aspects of vortex breakdown. *Prog. Aerospace Sci.* **30**, 1–59.

Delery, J. M., Horowitz, E., Leuchter, O. & Solignac, J. L. 1984 Fundamental studies on vortex flows. *La Recherche Aerospatiale* **2**, 1–24.

Erlebacher, G., Hussaini, M. Y. & Shu, C.-W. 1997 Interaction of a shock with a longitudinal vortex. *J. Fluid Mech.* **337**, 129–153.

Glotov, G. F. 1989 Interference of vortex braid with free-stream shock waves and nonisobaric jets. *TsAGI, Uchenye Zapiski* **20**, 21–32.

Hall, M. G. 1972 Vortex breakdown. *Ann. Rev. Fluid Mech.* **4**, 195–218.

https://doi.org/10.1017/S0022112098001566 Published online by Cambridge University Press

Kalkhoran, I. M. 1994 Vortex distortion during vortex-surface interaction in a Mach 3 stream. *AIAA J.* **32**, 123–129.

Kalkhoran, I. M., Smart, M. K. & Betti, A. 1996 Interaction of a supersonic wing tip vortex with a normal shock. *AIAA J.* **34**, 1855–1861.

Kandil, O. A. & Kandil, H. A. 1991 Supersonic quasi-axisymmetric vortex breakdown. *AIAA Paper* 91-3311.

Leibovich, S. 1984 Vortex stability and breakdown: Survey and extension. *AIAA J.* **22**, 1192–1206.

Mahesh, K. 1996 A model for the onset of breakdown in an axisymmetric compressible vortex. *Phys. Fluids* **8**, 3338–3345.

Metwally, O. & Settles, G. 1988 Measurements of a supersonic turbulent vortex. *Proc. 11th Symp. on Turbulence*, *University of Missouri*, *Rolla Missouri*.

Metwally, O., Settles, G. & Horstman, C. 1989 An experimental study of shock wave/vortex interaction. *AIAA Paper* 89-0082.

Nedungadi, A. & Lewis, M. J. 1996 Computational study of the flowfields associated with oblique shock/vortex interactions. *AIAA J.* **34**, 2545–2553.

Newsome, R. W. 1984 Numerical simulation of near-critical and unsteady, subcritical inlet flow. *AIAA J.* **22**, 1375–1379.

Paek, C. W. 1997 Measurements of flow properties in a supersonic wing-tip vortex. Masters thesis, Polytechnic University, Brooklyn New York.

Rizzetta, D. P. 1995 Numerical simulation of oblique shock-wave/vortex interaction. *AIAA J.* **33**, 1441–1446.

Rizzetta, D. P. 1997 Numerical simulation of vortex-induced shock-wave distortion. *AIAA J.* **35**, 209–211.

Sarpkaya, T. 1971 On stationary and travelling vortex breakdowns. *J. Fluid Mech.* **45**, 585–595.

Sarpkaya, T. 1995 Turbulent vortex breakdown. *Phys. Fluids* **7**, 2301–2303.

Smart, M. K. & Kalkhoran, I. M, 1995 The effect of shock strength on oblique shock wave-vortex interaction. *AIAA J.* **33**, 2137–2143.

Smart, M. K. & Kalkhoran, I. M. 1997 Flow model for predicting normal shock wave induced vortex breakdown. *AIAA J.* **35**, 1589–1596.

Smart, M. K., Kalkhoran, I. M. & Bentson, J. 1995 Measurements of supersonic wing tip vortices. *AIAA J.* **33**, 1761–1768.

Zatoloka, V., Ivanyushkin, A. K. & Nikolayev, A. V. 1978 Interference of vortexes with shocks in airscoops. Dissipation of vortexes. *Fluid Mech. Sov. Res.* **7**, 153–158.

https://doi.org/10.1017/S0022112098001566 Published online by Cambridge University Press